RESEARCH ARTICLE

MicroRNA and proteome expression profiling in early-symptomatic α-synuclein(A30P)-transgenic mice

Frank Gillardon[1], Matthias Mack[2], Wolfgang Rist[1], Cathrin Schnack[1], Martin Lenter[1], Tobias Hildebrandt[1] and Bastian Hengerer[1]

[1] Boehringer Ingelheim Pharma GmbH & Co. KG, Biberach an der Riss, Germany
[2] Mannheim University of Applied Sciences, Mannheim, Germany

Received: July 29, 2007
Revised: December 11, 2007
Accepted: December 13, 2007

The α-synuclein has been implicated in the pathophysiology of Parkinson's disease (PD), because mutations in the alpha-synuclein gene cause autosomal-dominant hereditary PD and fibrillary aggregates of alpha-synuclein are the major component of Lewy bodies. Since presynaptic accumulation of α-synuclein aggregates may trigger synaptic dysfunction and degeneration, we have analyzed alterations in synaptosomal proteins in early symptomatic α-synuclein(A30P)-transgenic mice by two-dimensional differential gel electrophoresis. Moreover, we carried out microRNA expression profiling using microfluidic chips, as microRNA have recently been shown to regulate synaptic plasticity in rodents and to modulate polyglutamine-induced protein aggregation and neurodegeneration in flies. Differentially expressed proteins in α-synuclein(A30P)-transgenic mice point to alterations in mitochondrial function, actin dynamics, iron transport, and vesicle exocytosis, thus partially resembling findings in PD patients. Oxygen consumption of isolated brain mitochondria, however, was not reduced in mutant mice. Levels of several microRNA (miR-10a, -10b, -212, -132, -495) were significantly altered. One of them (miR-132) has been reported to be highly inducible by growth factors and to be a key regulator of neurite outgrowth. Moreover, miR-132-recognition sequences were detected in the mRNA transcripts of two differentially expressed proteins. MicroRNA may thus represent novel biomarkers for neuronal malfunction and potential therapeutic targets for human neurodegenerative diseases.

Keywords:
MicroRNA / Parkinson / Synaptosome / Transgenic mice

1 Introduction

Parkinson's disease (PD) is diagnosed postmortem by the selective loss of dopaminergic neurons in the substantia nigra and the presence of intraneuronal protein deposits termed Lewy bodies. Biochemical analysis led to the identification of α-synuclein as a major component of Lewy bodies in PD brains. In the healthy brain, α-synuclein is abundantly expressed in central neurons and localizes to presynaptic terminals, where it may regulate synaptic vesicle mobilization. Certain point mutations in the α-synuclein gene cause autosomal-dominant hereditary Parkinson's disease (PD). The corresponding amino acid exchanges (A30P, E46K, A53T) favor aggregation of α-synuclein both *in vitro* and *in vivo* [1, 2]. Gene multiplications in the wild-type α-synuclein gene have also been linked to rare familial forms of PD. Although the pathomechanisms underlying familial and sporadic PD remain enigmatic, mitochondrial or proteasomal dysfunction and oxidative stress appear to be major contributors [1, 2]. Recent histological and biochemical analysis of brain samples revealed that about 90% of α-synuclein aggregates localize to presynaptic endings where they seem to affect synaptic structure and function [3]. Several transgenic mouse models overexpressing mutant α-synuclein

Correspondence: Dr. Frank Gillardon, Boehringer Ingelheim Pharma GmbH & Co. KG, CNS Research, Birkendorfer Str. 65, 88397 Biberach an der Riss, Germany
Fax: +49-7351-549-8928
E-mail: Frank.Gillardon@bc.boehringer-ingelheim.com

Abbreviations: **HMG-CoA**, 3-hydroxy-3-methyl-glutaryl-CoA; **MG-CoA**, 3-methylglutaconyl-CoA; **miRNA**, microRNA; **PD**, Parkinson's disease

have been generated that age-dependently exhibit α-synuclein immunoreactive intraneuronal inclusions, locomotor dysfunction and loss of dopaminergic synapses, thus partially mimicking PD [4, 5]. To gain insight into the mechanisms of α-synuclein-mediated neurotoxicity, we performed a brain proteome analysis of the α-synuclein(A30P)-transgenic mice mouse model for PD [6] using 2-D DIGE. Since aggregation of mutant α-synuclein may start within presynaptic terminals before being retrogradely transported and sequestered into somatic Lewy bodies [3], we focused on alterations in synaptosomal proteins in early symptomatic transgenic mice.

In addition, we performed a differential expression analysis for microRNA (miRNA) using microarray technology. MiRNA are non-coding transcripts of 19–24 nucleotides that are processed from double-stranded hairpin precursors by an RNase termed Dicer [7]. The mature single-stranded miRNA is then translocated to the RNA-induced silencing complex that suppresses translation of the target mRNA. Recent evidence indicates that in multicellular organisms, hundreds of miRNA can regulate the translation of about one third of the coding mRNA [7]. MiRNA have been shown to modulate stem-cell differentiation, hematopoiesis, muscle development, insulin secretion, cholesterol metabolism, and immune responses. Aberrant miRNA expression has been implicated in cancer and heart disease [8]. In the mammalian nervous system, expression of various miRNA increases during development and may influence neural patterning, cell specification and axonal path finding [7, 9]. In mature neurons, depolarization causes a sixfold increase in miR-134 expression. Brain-specific miR-134 seems to block translation of dendritic mRNA (*e.g.* LIM-domain kinase 1), thereby regulating synaptic plasticity and spine size [10]. Furthermore, growth factor treatment induced a rapid and persistent neuronal expression of miR-132 that promotes neurite outgrowth by targeting p250GAP, a regulator of Rho/Rac signaling [11]. Recent findings indicate that miRNA may also play a role in neurodegeneration [12]. General reduction of miRNA processing by knocking down Dicer activity massively enhances neurodegeneration in fruit flies that overexpress pathogenic Ataxin-3 or Tau protein [12]. Transgenic overexpression of miRNA *ban* suppressed neurodegeneration. Notably, *ban* overexpression did not alter aggregation of toxic proteins or execution of programmed cell death [12]. Taken together, changes in miRNA expression may represent a molecular signature of alterations in neuronal structure or function and may contribute to neuronal survival in the context of human neurodegenerative diseases [13, 14].

2 Materials and methods

2.1 Animals

Generation and characterization of homozygous (Thy1)-human α-synuclein(A30P)-transgenic mice (line 31H) have been described in detail elsewhere [6]. Age- and sex-matched, non-transgenic C57BL/6 mice were used as controls. All animal procedures were approved by the Federal Animal Care Committee.

2.2 Subcellular fractionation

Synaptosomal fractions were isolated by differential centrifugation using standard protocols. Enrichment of presynaptic marker proteins was assessed in previous studies [15, 16]. Briefly, mice (n = 4 *per* group) were killed by cervical dislocation followed by decapitation. The brains were rapidly removed and placed into ice-cold homogenization buffer containing 50 mM MOPS, pH 7.4, 320 mM sucrose, 0.2 mM DTT, 100 mM KCl, 0.5 mM $MgCl_2$, 0.01 mM EDTA, 1 mM EGTA, and phosphatase/protease inhibitor cocktails (Roche, Mannheim, Germany). All subsequent steps were performed at 4°C. The brains were cross-sectioned at Bregma -2.8 mm. The cerebellum was discarded. The cortex containing scattered proteinase K-resistant α-synuclein aggregates and the brainstem showing abundant histopathology at 12 months of age [6] were separately microdissected. Tissue samples were homogenized in 1:10 w/v homogenization buffer with 12 strokes in a Teflon-glass douncer. The homogenate was centrifuged for 10 min at $800 \times g$ followed by centrifugation of the supernatant at $9200 \times g$ for 15 min. The resulting pellet (P2), representing the crude synaptosomal fraction, and the supernatant (S2) were solubilized in lysis buffer containing 30 mM Tris, 8 M urea, 4% w/v CHAPS, pH 8.5 (GE Healthcare, Freiburg, Germany). Proteins in the S2 supernatant were precipitated using the 2D Clean-up Kit before solubilization as described in the manufacturer's protocol (GE Healthcare). Aliquots were taken for protein determination using the modified Bio-Rad protein assay (Bio-Rad, München, Germany) before freezing the samples at −80°C.

Metabolically active mitochondria were isolated using the Mitochondria Isolation Kit (Sigma, Taufkirchen, Germany) [16]. Mice (n = 3 *per* group) were killed and brain regions were microdissected as described above. Tissue samples were homogenized in 1:10 w/v ice-cold extraction buffer (200 mM mannitol, 1 mM EGTA, 70 mM sucrose, 2 mg/mL BSA, 10 mM HEPES, pH 7.5) using a Teflon-glass potter homogenizer (10 strokes, 400 rpm). All steps were performed at 4°C. The homogenate was centrifuged for 4 min at $1400 \times g$. The supernatant was subsequently centrifuged for 5 min at $30\,700 \times g$. The P2 pellet containing myelin, synaptosomes and mitochondria was resuspended in 2 mL extraction buffer and centrifuged for 3 min at $800 \times g$. The supernatant was again centrifuged for 5 min at $32\,500 \times g$ and the resulting pellet was resuspended in 120 μL extraction buffer. Aliquots were taken for determination of protein concentration using the Pierce BCA kit (Pierce, Bonn, Germany).

2.3 Mitochondrial respiration

Mitochondrial oxygen consumption was monitored in the mitochondrial fractions using an Oxygraph-2k system which is equipped with two chambers and polarographic oxygen sensors (Oroboros, Innsbruck, Austria) [16, 17]. Mitochondria (0.4 mg at 1 mg/mL) were incubated at 25°C in respiration buffer (100 mM KCl, 1 mM $MgCl_2$, 75 mM mannitol, 25 mM sucrose, 1 mM KH_2PO_4, 0.5 mg/mL BSA, 10 mM Tris-HCl, pH 7.4). Oxygen consumption was initiated by administration of pyruvate and malate (5 mM each). Thereafter, state 3 respiration was triggered by administration of ADP (375 μM). Carbonylcyanide-4-(trifluoromethoxy)-phenylhydrazone (FCCP, 1 μM) was then added to measure uncoupled respiration. Rotenone (5 μM) was subsequently administered to inhibit complex I activity. Finally, the complex II substrate succinate was added (5 mM) and respiration measurement was completed. Values were normalized to protein content.

2.4 Gel electrophoresis and immunoblotting

The 2-D DIGE was performed according to the manufacturer's instructions (GE Healthcare) with minor modifications [18, 19]. In short, samples (four biological replicates *per* group) in lysis buffer were set to a protein concentration of 2 μg/μL and centrifuged at $12\,000 \times g$ for 10 min to remove insoluble material. Proteins (50 μg/sample) were labeled with 400 pmol Cy3 or Cy5 cyanine dye. As internal standard aliquots of each sample were pooled and labeled with Cy2 dye. To exclude preferential labeling of the dyes, samples were also reverse labeled. The two differentially labeled samples plus the internal standard were combined and an equal volume of 2x sample buffer (8 M urea, 4% w/v CHAPS, 2% w/v DTT, 2% v/v Pharmalyte) was added. Finally, DeStreak Rehydration solution (plus 0.5% v/v Pharmalyte) was added to a final volume of 450 μL. IPG strips (Immobiline DryStrip, 24 cm, pH 3–10 NL, GE Healthcare, Germany) were rehydrated in the presence of protein samples for 12 h at 30 V. IEF was performed using an Ettan IPGphor (GE Healthcare) at a maximum current of 50 μA/strip as follows: 300 V for 3 h, 1000 V for 6 h, and 8000 V for 7 h. Following equilibration, the IPG strips were placed on top of 12.5% polyacrylamide gels. SDS polyacrylamide gel electrophoresis was conducted overnight in an Ettan DALT twelve electrophoresis system (GE Healthcare) at 20 mA/gel and 20°C in a buffer containing 25 mM Tris, 192 mM glycine, and 0.2% w/v SDS. The 2-D DIGE was performed twice (two gel replicates/sample) generating similar results. NEPHGE, pH 3–10 NL (four independent biological replicates *per* group) was performed by Wita (Teltow, Germany).

All gels were scanned between the low-fluorescent glass plates using a Typhoon 9400 laser scanner (GE Healthcare). Gel images were analyzed automatically using DeCyder software version 5.0 (Differential In-gel Analysis and Biological Variation Analysis) (GE Healthcare), which performs spot detection, in-gel normalization, spot matching, and statistical analysis of protein abundance levels between different gels. Software algorithms and statistical confidence are described in detail by others [20]. Protein spots of interest were excised from the gels using an Ettan Spot Picker robot (GE Healthcare). Gel pieces were incubated in 100 μL ACN for 5 min and subsequently dried in a vacuum centrifuge. Gel pieces were rehydrated with 5 μL of 50 mM ammonium bicarbonate containing 20 ng/μL trypsin (sequencing grade, Promega, Mannheim, Germany) for 30 min at 4°C. Thereafter, proteins were digested overnight at 37°C. The resulting peptides were eluted with 20 μL of 0.1% v/v TFA by sonication for 15 min.

Proteins (20 μg/lane) were separated on 12% polyacrylamide minigels and subsequently transferred to nitrocellulose membranes using a wet transfer system (Bio-Rad, München, Germany). After blocking in buffer containing 20 mM Tris, pH 7.4, 500 mM NaCl, 0.1% Tween 20, and 5% BSA for 90 min, the membranes were incubated overnight with an affinity-purified sheep polyclonal antibody against transferrin (1 μg/mL, Bethyl Laboratories, Montgomery, TX). HRP-conjugated secondary antibodies and enhanced chemiluminescence reagents (ECL kit; GE Healthcare) were used for detection. Membranes were checked for protein load and protein transfer using a commercial kit (MemCode Reversible Protein Stain Kit, Pierce, Rockford, IL) that reversibly stains for total protein. Densitometric analysis of immunoblots was performed using Quantity One (Bio-Rad).

2.5 MS

MS/MS analysis was performed with an UltiMate nanoHPLC system (LC Packings, Amsterdam, Netherlands) connected to a QSTAR XL quadrupole TOF hybrid mass spectrometer (ABI Sciex, Toronto, Canada) [21]. The dried peptide sample was dissolved in 10 μL of 2% ACN, 0.1% TCA, applied to a precolumn (PepMap C18, 0.3×5 mm) (Dionex, Idstein, Germany) and separated using an analytical column (PepMap C18, 0.075×150 mm) (Dionex) at a flow rate of 250 nL/min. The mobile phases were A = 2% ACN, 0.1% formic acid and B = 80% ACN, 0.1% formic acid. The gradient for separation was 5–50% B in 30 min, 50–100% B in 2 min. A survey scan from m/z 350 to 1300 was performed for 1 s with subsequent two MS/MS scans for 2 s each. Precursor ions were dynamically excluded for 120 s. Under script control (Analyst, ABI Sciex) the acquired product ion spectra were submitted to the MASCOT database search engine (Matrix Science, London, UK) against the Swiss-Prot database with the following search parameters: maximum of one missed trypsin cleavage, cysteine carbamidomethylation, methionine oxidation, and a maximum 0.20 Da error tolerance in both the MS and MS/MS data. All hits were manually verified using accepted rules for peptide fragmentation [21].

2.6 Assay of 3-methylglutaconyl-CoA hydratase

Brainstem tissue samples were suspended in 200 μL PBS by repeated pipetting and sonicated three times on ice for 15 s at 8 W at 45-s intervals. An aliquot of the homogenate (5–7 μg) was added to the 3-methylglutaconyl-CoA hydratase assay. Protein was estimated using the method of Bradford (Bio-Rad). The hydratase assay mixture contained, in a final volume of 25 μL, 100 mM Tris-HCl pH 8.0, 10 mM EDTA, 1 mg/mL BSA and 10 μM 3-methylglutaconyl-CoA or glutaconyl-CoA. After incubation at 37°C for 60 min, the reaction was terminated by the addition of 2.5 μL of 2 mM HCl. The samples were homogenized and the assay tubes were placed on ice. After 5 min, the homogenates were brought to pH 6 with 2 mM KOH, 1 mM MES pH 6 and centrifuged at $21\,000 \times g$ for 10 min at 4°C. The supernatant was transferred to an HPLC vial. The products of the reaction, 3-hydroxy-3-methylglutaryl-CoA, or 3-hydroxyglutaryl-CoA were detected at 260 nm using the HPLC system as described previously [22].

2.7 MicroRNA expression analysis

MiRNA expression profiling was performed using LC Sciences microfluidic chip technology (LC Sciences, Houston, TX). Briefly, mice ($n = 3$ *per* group) were killed by decapitation, the brains were rapidly removed and the brainstems were microdissected as described above. Brainstem tissue samples were homogenized and total RNA was extracted using Trizol reagent according to the manufacturer's protocol (Invitrogen, Paisley, UK) with minor modifications. In brief, RNA was precipitated using 1.5 mL isopropyl alcohol/1 mL of Trizol reagent. The extracts were incubated at -20°C overnight and subsequently centrifuged at $12\,000 \times g$ for 10 min at 4°C to precipitate low-molecular weight RNA. The RNA pellets were resuspended in RNase-free water for OD measurements. OD 260 nm/280 nm ratios were all above 1.8 and OD 260 nm/230 nm ratios were above 1.5. Following administration of three volumes of 100% ethanol, 1/10 volume of 3 M NaOAc, pH 4.8, and 10 μM EDTA, samples were shipped on dry ice to LC Sciences for chip analysis. Chip design, assay protocol, and data analysis are described in detail elsewhere (www.lcsciences.com). Total RNA samples (10 μg each) were size fractionated using a YM-100 Microcon centrifugal filter (Millipore, Bedford, MA) and the small RNA (<300 nt) were 3'-extended with a poly(A) tail using poly(A) polymerase. An oligonucleotide tag was then ligated to the poly(A) tail for fluorescent dye staining. RNA samples from α-synuclein(A30P)-transgenic and control mice were labeled with green-fluorescent Cy3 dye and red-fluorescent Cy5 dye, respectively. Both samples were then hybridized to the same μParaflo microfluidic chip (#MRA-1002) (LC Sciences) containing 266 unique mature mouse miRNA probes in triplicate. On the microfluidic chip, each detection probe consisted of a chemically modified nucleotide coding segment complementary to target miRNA (from miRBase, http://microrna.sanger.ac.uk/sequences/) and a spacer segment of polyethylene glycol to extend the coding segment away from the substrate. The detection probes were made by *in situ* synthesis using photogenerated reagent chemistry. The hybridization melting temperatures were balanced by chemical modifications of the detection probes. Hybridization used 100 μL 6 x SSPE buffer (0.90 M NaCl, 60 mM Na_2HPO_4, 6 mM EDTA, pH 6.8) containing 25% formamide at 34°C. After hybridization, fluorescence images were collected using a laser scanner (GenePix 4000B, Molecular Devices, Sunnyvale, CA) and digitized using Array-Pro image analysis software (Media Cybernetics, Bethesda, MD). Data were analyzed by first subtracting the background and then normalizing the signals. Finally, the ratio of the Cy3/Cy5 signals (log2 transformed) and *p*-values of the *t*-test were calculated. Differentially detected signals were those with *p*-values <0.01.

2.8 Gene expression profiling

Affymetrix (Affymetrix, Santa Clara, CA) genechip (HG-U133AB) analysis was performed by Gene Logic (Gene Logic, Gaithersburg, MD) using human postmortem brain samples.

3 Results

3.1 Proteome analysis

Using 2-D DIGE analysis of murine brainstem tissue, we detected about 1000 spots *per* gel. Protein spots that were present in all gels (four biological replicates *per* group) and showed statistically significant differences ($p<0.05$, *t*-test, DeCyder, Biological Variation Analysis) were selected for further analysis. By these criteria, 11 spots were found to be differentially expressed in α-synuclein(A30P) overexpressing mice compared to non-transgenic controls. Three spots were very faint and thus could not be identified unambiguously by MS. Seven differentially expressed proteins were identified in the P2/S2 fractions and are listed in Table 1. Magnified sections of representative gel images are shown in Fig. 1. The two transferrin spots at p*I* values of 6.2 and 6.0 (Fig. 1) may represent apotransferrin and monoferric transferrin as shown by others [23]. In order to increase detection of membrane proteins and spot resolution [24], we analyzed the synaptosomal P2 fraction (four independent biological replicates *per* group) also by NEPHGE and used second dimension gels 24×30 cm in size (Supporting Information Fig. 1). However, additional deregulated synaptosomal proteins were not detected by NEPHGE.

By immunoblotting using a commercially available anti-transferrin antibody and densitometric analysis we verified a significant increase in transferrin (194 ± 21% of non-transgenic controls, mean ± SD) in brainstem lysates of α-synuclein(A30P) overexpressing mice (Fig. 2). Notably, two mito-

Table 1. Changes in brainstem protein levels in alpha-synuclein(A30P)-transgenic mice compared to wild-type animals

Protein	Accession no.	Average ratio[a)]	MASCOT score	Sequence-coverage (%)
Brainstem P2 fraction				
Methylglutaconyl-CoA hydratase, mitochondrial precursor	Q9JLZ3	−1.94	250	17.5
ATP synthase alpha chain, mitochondrial precursor	QO3265	−1.52	393	13.0
LIM and SH3 domain protein (LASP-1)	Q61792	+1.21	184	15.0
Vesicle-fusing ATPase	P18708	+1.29	203	10.5
Brainstem S2 fraction				
Methylglutaconyl-CoA hydratase, mitochondrial precursor	Q9JLZ3	−1.95	197	17.0
Sorting nexin-12 (SDP8 protein)	O70493	+1.45	213	33.0
Ubiquitin-conjugating enzyme E2 L3	P68037	+1.45	144	29.0
Serotransferrin precursor (Transferrin)	Q921I1	+1.30	1020	46.0
LIM and SH3 domain protein (LASP-1)	Q61792	+1.21	283	11.5

a) Average ratio: negative values indicate decreased protein levels in transgenic mice.

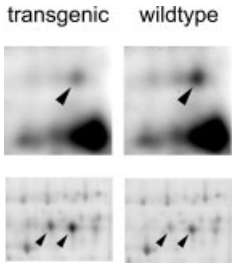

Figure 1. 2-D DIGE of brainstem synaptosome fractions from α-synuclein(A30P)-transgenic mice (left panels) and wild-type animals (right panels). Magnified sections from representative gel images showing the decrease in 3-methylglutaconyl-CoA hydratase (upper row, arrowhead) and the increase in transferrin (lower row, arrowheads) in transgenic mice.

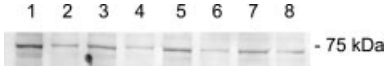

Figure 2. Immunoblot analysis of transferrin levels in brainstem S2 fractions. An increase in transferrin is detectable in lysates of four α-synuclein(A30P) overexpressing mice (lanes 1, 3, 5, 7) compared to wild-type controls (lanes 2, 4, 6, 8).

chondrial proteins were significantly down-regulated in mutant mice as compared to controls. ATP synthase (EC 3.6.3.14) is involved in mitochondrial oxidative phosphorylation and 3-methylglutaconyl-CoA hydratase (EC 4.2.1.18) (Fig. 1) is active in mitochondrial energy metabolism.

Affymetrix genechip (HG-U133AB) analysis revealed an age-dependent decline in 3-methylglutaconyl-CoA hydratase mRNA levels in the human brain. More importantly, a significant ($p<0.05$, ANOVA) reduction in 3-methylglutaconyl-CoA hydratase mRNA expression by approximately 20% was also observed in several brain areas of PD patients (*e.g.* substantia nigra, caudate nucleus, nucleus ambiguus, putamen, frontal cortex) compared to age-matched controls ($n\geq10$ samples each).

3.2 Respiration of isolated mitochondria

Impairment of mitochondrial oxidative phosphorylation has been reported in PD and pharmacological inhibition causes a Parkinsonian phenotype in animal models [2]. To analyze the functional significance of mitochondrial proteome alterations, we monitored the respiration rate of crude mitochondrial preparations using the Oxygraph-2k system (Oroboros). As shown in Fig. 3A, basal mitochondrial respiration in the presence of malate and pyruvate did not differ between α-synuclein(A30P) overexpressing mice and control animals (n = 3 *per* group). ADP-stimulated state 3 respiration and FCCP-triggered uncoupled respiration were also unchanged in mitochondria purified from brainstem tissue.

3.3 3-Methylglutaconyl-CoA hydratase activity

Protein levels of 3-methylglutaconyl-CoA hydratase declined by approximately 50% in α-synuclein(A30P)-transgenic mice (Table 1). In order to also monitor enzyme function, we tested brainstem extracts (n = 3 *per* group) for hydratase activity using two different substrates, 3-methylglutaconyl-CoA and glutaconyl-CoA. However, 3-methylglutaconyl-CoA hydratase activity was below the detection limit of our assay probably due to the very low amounts of enzyme present in the extracts (Fig. 1).

3.4 MicroRNA expression analysis

Small RNA isolated from α-synuclein(A30P)-transgenic and control mice brainstem tissue (n = 3 *per* group) were labeled with green-fluorescent Cy3 dye and red-fluorescent Cy5 dye, respectively. Both samples were then hybridized to the same microfluidic chip containing 266 unique mouse miRNA probes in triplicate. The RNA extracts were of good quality and produced strong signals on the chips with low noise levels. Figure 3B displays representative regions of chip

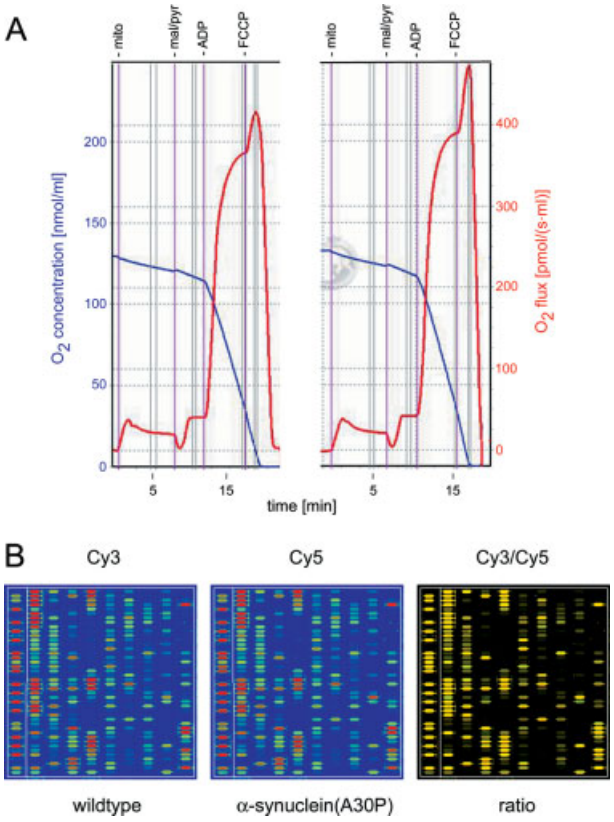

Figure 3. (A) Representative measurements of mitochondrial oxygen consumption (oxygen flux is shown in red on the right vertical axis; oxygen concentration is shown in blue). Mitochondria-enriched fractions were prepared from the mouse brainstem and administered into the Oxygraph-2k analytical chamber (mito). Basal respiration after adding malate/pyruvate (mal/pyr) did not significantly differ between α-synuclein(A30P)-transgenic mice (right panel) and wild-type animals (left panel). ADP stimulated state 3 respiration and FCCP triggered uncoupled respiration reflecting mitochondrial respiratory capacity were also unchanged. (B) Representative regions of microRNA chip images. The Cy3 and Cy5 intensity images are color-coded. Red signals indicate miRNA that are highly expressed in the mouse brainstem. In the Cy3/Cy5 ratio image the color is yellow when Cy3 (wild-type mouse microRNA) level is equal to Cy5 (mutant α-synuclein-transgenic mouse microRNA) level. The color is green when Cy3 level is higher than Cy5 level. The color is red when Cy3 level is lower than Cy5 level.

images. The Cy3 and Cy5 intensity images are pseudo-colored. As the signal intensity increases from 1 to 55 000, the corresponding color changes from blue to green, to yellow, and to red. Red signals indicate miRNA that are expressed at high levels in the mouse brainstem. Brainstem-enriched miRNA with averaged signal intensities higher than 20 000 included miR-7a, -7b, -7c, -7d, -7e, -7f, -7g, -7i, -9, -9*, -16, -21, -23a, -23b, -27b, -26a, -26b, -29a, -29b, -29c, -30a-5p, -30b, -30c, -30d, -98, -124a, -124b, -125b, -125b, -126-3p, -128a, -128b, -132, -181a, -218, -434-3p, and -709. In the Cy3/Cy5 ratio image (Fig. 3B), the color is yellow when Cy3 (wild-type mouse miRNA) level is equal to Cy5 (mutant α-synuclein-transgenic mouse miRNA) level. The color is green when Cy3 level is higher than Cy5 level. The color is red when Cy3 level is lower than Cy5 level. MiRNA that were modulated on three chips with a p-value <0.01 were considered differentially expressed and are listed in Table 2. Signal intensities of miR-10a, and -10b are low, indicating that these miRNA are weakly expressed in the murine brainstem, whereas miR-212, -495, and -132 are present at moderate to high levels. Although the miRNA listed in Table 2 were all down-regulated, there was no general decline in miRNA expression in the brainstems of mutant α-synuclein overexpressing mice.

Using computational target prediction algorithms (miRanda, miRBase, Targetscan) we could identify sortin nexin-12 and ubiquitin-conjugating enzyme E2 as potential targets for miR-132 as has been reported by others [25, 26]. The increase in these proteins in the brainstem of our mutant α-synuclein-transgenic mice shown by 2-D DIGE analysis (Table 1) would be consistent with the decline in miR-132 levels detected on microchips (Table 2).

Table 2. Changes in brainstem microRNA levels in alpha-synuclein(A30P)-transgenic mice (Cy5 signal) compared to wild-type mice (Cy3 signal)

Probe_ID	Cy3 signal	Cy5 signal	Log2 (Cy5/Cy3)
mmu-miR-10b	592	210	−1.4
mmu-miR-10a	656	326	−0.9
mmu-miR-212	5339	3408	−0.6
mmu-miR-132	27 598	19 052	−0.5
mmu-miR-495	12 214	9114	−0.5

4 Discussion

In the human α-synuclein(A30P)-transgenic mouse model for PD, behavioral impairment and α-synuclein aggregation starts at approximately 12 months of age [6]. In a recent study using 2-DE, oxidative modifications in two glycolytic enzymes were detected in α-synuclein(A30P)-transgenic mice brains compared to non-transgenic controls [27]. In this study, however, end-stage mice and total brain homogenates were analyzed. In order to detect early pathogenic events within vulnerable compartments, we tested α-synuclein (A30P) overexpressing mice at the onset of motor dysfunction, microdissected brainstem tissue and enriched the synaptosomal fraction, where aggregated α-synuclein may exert its pathogenic effects [3, 6]. Using 2-D DIGE, we detected changes in proteins involved in mitochondrial function, iron transport, actin dynamics, and vesicle exocytosis. Lack of neuronal cell loss and absence of glial activation in our transgenic mouse model might explain why these alterations in protein levels were only moderate ranging from −50 to +45%. Changes in actin cytoskeletal proteins

and mitochondrial proteins (*e.g.* ATP synthase subunits) were also detected in proteomic studies analyzing heads from early symptomatic α-synuclein(A30P)-transgenic *Drosophila melanogaster* [28] and autopsy brain tissue from sporadic PD patients, respectively [29]. Isotope-coded affinity tag-based analysis of mitochondria-enriched fractions from nigral tissue revealed 119 differentially-expressed proteins in PD patients, including subunits of the mitochondrial electron transport complexes [30]. Detailed immunoblot analysis of the electron transport complexes demonstrated specific changes in complex I subunit composition in the PD frontal cortex [31]. Although these proteomic data point to similar functional defects in patients and animal models, there is only minor overlap in the proteins identified.

Mitochondrial dysfunction seems to play a central role in PD and a significant reduction in mitochondrial complex I catalytic activity has been shown in brain tissue of sporadic PD patients [2, 31]. In our study, respiration of mitochondria enriched from brainstem tissue did not differ between early symptomatic (12-months-old) α-synuclein(A30P)-transgenic mice and controls. Consistently, unchanged brain mitochondrial respiration was recently reported in two mouse lines that overexpress double mutant α-synuclein(A30P/A53T) [32]. On the other hand, mitochondrial complex IV activity declined by about 80% in the spinal cord of symptomatic α-synuclein(A53T)-transgenic mice. In contrast to the aforementioned mouse lines, this line exhibits a massive loss of central neurons [33].

The factors underlying differences in vulnerability remain enigmatic. Our proteomic data do not show a compensatory up-regulation of potential neuroprotective proteins (*e.g.* HSP, glycolytic enzymes), whereas protein levels of mitochondrial ATP synthase alpha chain and 3-methylglutaconyl-CoA (MG-CoA) hydratase significantly decreased in the mutant mice. In order to monitor enzyme function, we tested brainstem extracts for MG-CoA hydratase activity [22]. However, catalytic activity was below the detection limit of our assay probably due to the very low amounts of enzyme present in the mouse brainstem extracts. On the other hand, mRNA levels of MG-CoA hydratase were also reduced in affected brain regions of PD patients pointing to a pathophysiological function. MG-CoA hydratase catalyses the hydration of MG-CoA to 3-hydroxy-3-methyl-glutaryl-CoA (HMG-CoA) in the leucine degradation pathway. HMG-CoA is then converted to acetoacetate and acetyl-CoA [22]. Reduced mitochondrial MG-CoA hydratase activity in humans results in psychomotor retardation with progressive neurological symptoms. The ketone bodies acetoacetate and 3-hydroxybutyrate represent a major alternative to glucose as energy substrate in the mammalian brain. Moreover, administration of ketone bodies protected cultured midbrain neurons against the mitochondrial complex I inhibitor MPP+ and increased survival of α-synuclein(A53T)-transgenic *Caenorhabditis elegans* exposed to rotenone [34, 35].

A pivotal role of iron-mediated free radical stress has been emphasized in PD and transcranial sonography has demonstrated iron accumulation in the substantia nigra of early symptomatic familial and sporadic PD patients [36, 37]. Extracellular iron is bound to transferrin and is internalized by cells *via* the transferrin receptor. The significant increase in brainstem transferrin levels in our α-synuclein(A30P) overexpressing mice may be indicative of an enhanced iron uptake. Sorting nexin-12 (SNX12) is a member of the SNX3/Grd19 group of cellular trafficking proteins [38]. Notably, SNX3 is involved in transport of internalized transferrin receptors to recycling endosomes and of epidermal growth factor receptors to lysosomes. LIM and SH3 domain protein (LASP-1) is an actin-associated protein that is concentrated at neuronal synapses where it may be involved in actin cytoskeleton reorganization contributing to synaptic plasticity [39]. LASP-1 also binds to dynamin, which is critically required for synaptic vesicle endocytosis [40, 41]. Vesicle-fusion ATPase (also known as N-ethylmaleimide-sensitive fusion protein) is broadly required for intracellular membrane fusion including calcium-sensitive synaptic vesicle exocytosis [42]. Interestingly, alterations in epidermal growth factor receptor trafficking and synaptic vesicle dynamics have been detected in Parkin-deficient cells and α-synuclein (A30P) overexpressing neurons, respectively [43, 44].

Our miRNA expression analysis led to the identification of numerous brainstem-enriched miRNA. More importantly, we demonstrate for the first time that miRNA expression changes in a transgenic mouse model for PD in the absence of neuronal cell loss. Recent studies in cultured primary neurons demonstrated that expression of miR-132 significantly increases following growth factor administration or neuronal depolarization [11, 25]. Transfection with miR-132 expression vectors enhances neuronal excitability by glutamate [25]. The decline in miR-132 levels in our α-synuclein(A30P)-transgenic mice may thus represent a molecular signature for a concomitant decrease in neurotrophic support and/or neuronal activity in the affected brainstem. Moreover, the decrease in miR-132 may contribute to the increased expression of its predicted targets sortin nexin-12 and ubiquitin-conjugating enzyme E2 [25, 26]. After submission of this manuscript, Kim and coworkers reported a decrease of miR-133b in midbrain samples from PD patients [45]. MiRNA-133b modulates the differentiation of embryonic rat dopaminergic neurons in culture by targeting the transcription factor Pitx3 [45]. It will be important to identify and validate the mRNAs targets of miR-132, -133b, -212, and -495 in the ageing brain. Recent evidence suggests that miRNA might be drug targets for the treatment of human diseases and can be specifically blocked *in vivo* [46]. Thus, analysis of miRNA expression in biopsy specimen from diseased human brain combined with target mRNA identification may provide new therapeutic options.

The authors thank Sandra Felk, Susanne Zach, and Jessica Bretzel for excellent technical assistance. We also thank Dr. Carina Ittrich for help with genechip data analysis. We are grateful to

Prof. Christian Haass and Prof. Philipp Kahle for providing breeding pairs of mutant α-synuclein transgenic mice. This project was in part supported by the Landesstiftung Baden-Württemberg (P-LS-Prot/42).

The authors have declared no conflict of interest.

5 References

[1] Shults, C. W., Lewy bodies. *Proc. Natl. Acad. Sci. USA* 2006, *103*, 1661–1668.

[2] Dawson, T. M., Dawson, V. L., Molecular pathways of neurodegeneration in Parkinson's disease. *Science* 2003, *302*, 819–822.

[3] Kramer, M. L., Schulz-Schaeffer, W. J., Presynaptic α-synuclein aggregates, not Lewy bodies, cause neurodegeneration in dementia with Lewy bodies. *J. Neurosci.* 2007, *27*, 1405–1410.

[4] Dawson, T. M., Mandir, A. S., Lee, M. K., Animal models of PD: pieces of the same puzzle? *Neuron* 2002, *35*, 219–222.

[5] Melrose, H. L., Lincoln, S. J., Tyndall, G. M., Farrer, M. J. Parkinson's disease: a rethink of rodent models. *Exp. Brain Res.* 2006, *173*, 196–204.

[6] Freichel, C., Neumann, M., Ballard, T., Müller, V. *et al.*,. Age-dependent cognitive decline and amygdala pathology in a-synuclein transgenic mice. *Neurobiol. Ageing*, 2007, *28*, 1421–1435.

[7] Kosik, K. S., The neuronal microRNA system. *Nature Rev. Neurosci.* 2006, *7*, 911–919.

[8] Williams, A. E., Functional aspects of animal microRNAs. *Cell. Mol. Life Sci.* 2008, *65*, 545–562.

[9] Miska, E. A., Alvarez-Saavedra, E., Townsend, M., Yoshii, A. *et al.*, Microarray analysis of microRNA expression in the developing mammalian brain. *Genome Biol.* 2004, *5*, R68.

[10] Schratt, G. M., Tuebing, F., Nigh, E. A., Kane, C. G. *et al.*, A brain-specific microRNA regulates dendritic spine development. *Nature* 2006, *439*, 283–289.

[11] Vo, N., Klein, M. E., Varlamova, O., Keller, D. M. *et al.*, A cAMP-response element binding protein-induced microRNA regulates neuronal morphogenesis. *Proc. Natl. Acad. Sci. USA* 2005, *102*, 16426–16431.

[12] Bilen, J., Liu, N., Burnett, B. G., Pittman, R. N., Bonini, N. M., MicroRNA pathways modulate polyglutamine-induced neurodegeneration. *Mol. Cell* 2006, *24*, 157–163.

[13] Ashraf, S. I., Kunes, S., A trace of silence: memory and microRNA at the synapse. *Curr. Opin. Neurobiol.* 2006, *16*, 535–539.

[14] Bilen, J., Liu, N., Bonini, N. M., A new role for microRNA pathways. Modulation of degeneration induced by pathogenic human disease proteins. *Cell Cycle* 2006, *5*, 2835–2838.

[15] Luabeya, M. K., Vanisberg, M. A., Jeanjean, A. P., Baudhuin, P. *et al.*, Fractionation of human brain by differential and isopynic equilibration techniques. *Brain Res. Protocols* 1997, *1*, 83–90.

[16] Gillardon, F. G., Rist, W., Kussmaul, L., Vogel, J. *et al.*, Proteomic and functional alterations in brain mitochondria from Tg2576 mice occur before amyloid plaque deposition. *Proteomics* 2007, *7*, 605–616.

[17] Gnaiger, E., Bioenergetics at low oxygen: dependence of respiration and phosphorylation on oxygen and adenosine diphosphate supply. *Respir. Physiol.* 2001, *128*, 277–297.

[18] Tonge, R., Shaw, J., Middleton, B., Rowlinson, R. *et al.*, Validation and development of fluorescence two-dimensional gel electrophoresis proteomics technology. *Proteomics* 2001, *1*, 377–396.

[19] Viswanathan, S., Ünlü, M., Minden, J. S., Two-dimensional difference gel electrophoresis. *Nat. Protoc.* 2006, *1*, 1351–1358.

[20] Friedman, D. B., Quantitative proteomics for two-dimensional gels using difference gel electrophoresis. *In: Matthiesen, R. (Ed.), Methods in Molecular Biology,* Humana Press Totowa, NJ, 2007, vol. 367.

[21] Boldt, K., Rist, W., Weiss, S. M., Weith, A., Lenter, M. C., FPRL-1 induces modifications of migration-associated proteins in human neutrophils. *Proteomics* 2006, *6*, 4790–4799.

[22] Mack, M., Schniegler-Mattox, U., Peters, V., Buckel, W. *et al.*, Biochemical characterization of human 3-methylglutaconyl-CoA hydratase and ist role in leucine metabolism. *FEBS J.* 2006, *273*, 2012–2022.

[23] Richards, M. P., Huang T. L., Metalloprotein analysis by capillary isoelectric focusing. *J. Chromatogr. B. Biomed. Sci. Appl.* 1997, *690*, 43–54.

[24] Nowalk, A. J., Nolder, C., Clifton, D. R., Carroll, J. A., Comparative proteome analysis of subcellular fractions from *Borrelia burgdorferi* by NEPHGE and IPG. *Proteomics* 2006, *6*, 2121–2134.

[25] Cheng, H. M., Papp, J. W., Varlamova, O., Dziema, H. *et al.*, microRNA modulation of circadian-clock period and entrainment. *Neuron* 2007, *54*, 813–829.

[26] John, B., Enright, A. J., Aravin, A., Tuschl, T. *et al.*, Human microRNA targets. *PloS Biology* 2004, *2*, 1862–1879.

[27] Poon, H. F., Fraisier, M., Shreve, N., Calabrese, V. *et al.*, Mitochondrial associated metabolic proteins are selectively oxidized in A30P α-synuclein transgenic mice – a model of familial Parkinson's disease. *Neurobiol. Dis.* 2005, *18*, 492–498.

[28] Xun, Z., Sowell, R. A., Kaufman, T. C., Clemmer, D. E. Protein expression in a Drosophila model of Parkinson's disease. *J. Proteome Res.* 2007, *6*, 348–357.

[29] Basso, M., Giraudo, S., Corpillo D., Bergamasco, B. *et al.*, Proteome analysis of human substantia nigra in Parkinson's disease. *Proteomics* 2004, *4*, 3943–3952.

[30] Jin, J., Hulette, C., Wang, Y., Zhang, T. *et al.*, Proteomic identification of a stress protein, mortalin/mthsp70/Grp75. Relevance to Parkinson disease. *Mol. Cell. Proteomics* 2006, *5*, 1193–1204.

[31] Keeney, P. M., Xie, J., Capaldi, R. A., Bennett, J. P. Parkinson's disease brain mitochondrial complex I has oxidatively damaged subunits and is functionally impaired and misassembled. *J. Neurosci.* 2006, *26*, 5256–5264.

[32] Stichel, C. C., Zhu, X., Bader, V., Linnartz, B. *et al.*, Mono- and double-mutant mouse models of Parkinson's disease display severe mitochondrial damage. *Hum. Mol. Gen.* 2007, *16*, 3377–3393.

[33] Martin, L. J., Pan, Y., Price, A. C., Sterling, W. *et al.*, Parkinson's disease α-synuclein transgenic mice develop neuronal

mitochondrial degeneration and cell death. *J. Neurosci.* 2006, *26*, 41–50.

[34] Kashiwaya, Y., Takeshima, T., Mori, N., Clarke, K., Veech, R. L., D-β-hydroxybutyrate protects neurons in models of Alzheimer's and Parkinson's disease. *Proc. Natl. Acad. Sci. USA* 2000, *97*, 5440–5444.

[35] Ved, R., Saha, S., Westlung, B., Perier, C. *et al.*, Similar patterns of mitochondrial vulnerability and rescue induced by genetic modification of α-synuclein, parkin, and DJ-1 in Caenorhabditis elegans. *J. Biol. Chem.* 2005, *280*, 42655–42668.

[36] Berg, D., Gerlach, M., Youdim, M. B. H., Double, K. L. *et al.*, Brain iron pathways and their relevance to Parkinson's disease. *J. Neurochem.*, 2001, *79*, 225–236.

[37] Schweitzer, K. J., Brüssel, T., Leitner, P., Krüger, R. *et al.*, Transcranial ultrasound in different monogenetic subtypes of Parkinson's disease. *J. Neurol.*, 2007, in press.

[38] Worby, C. A., Dixon, J. E., Sorting out the cellular functions of the sorting nexins. *Nat. Rev. Mol. Cell Biol.* 2002, *3*, 919–931.

[39] Phillips, G. R., Anderson, T. R., Florens, L., Gudas, C. *et al.*, Actin-binding proteins in a postsynaptic preparation: Lasp-1 is a component of central nervous system synapses and dendritic spines. *J. Neurosci. Res.* 2004, *78*, 38–48.

[40] Okamoto, C. T., Li, R., Zhang, Z., Jeng, Y. Y., Chew, C. S., Regulation of protein and vesicle trafficking at the apical membrane of epithelial cells. *J. Contr. Release* 2002, *78*, 35–41.

[41] Robinson, P. J., How to fill a synapse. *Science* 2007, *316*, 551–553.

[42] Zhao, C., Slevin, J. T., Whiteheart, S. W., Cellular functions of NSF: not just SNAPs and SNAREs. *FEBS Lett.* 2007, *581*, 2140–2149.

[43] Fallon, L., Belanger, C. M. L., Corera, A. T., Kontogiannea, M. *et al.*, A regulated interaction with UIM protein Eps15 implicates parkin in EGF receptor trafficking and PI(3)K-Akt signaling. *Nat. Cell Biol.* 2006, *8*, 834–842.

[44] Gitler, A. D., Shorter, J., Prime time for α-synuclein. *J. Neurosci.*, 2007, *27*, 2433–2434.

[45] Kim, J., Inoue, K., Ishii, J., Vanti, W. B. *et al.*, A microRNA feedback circuit in midbrain dopamine neurons. *Science* 2007, *317*, 1220–1224.

[46] Hammond, S. M., MicroRNA therapeutics: a new niche for antisense nucleic acids. *Trends Mol. Med.* 2006, *12*, 99–101.

